Reversible intracellular translocation of KRas but not HRas in hippocampal neurons regulated by Ca^{2+}/calmodulin

Marc Fivaz and Tobias Meyer

Department of Molecular Pharmacology, Stanford University School of Medecine, Stanford, CA 94305

The Ras/MAPK pathway regulates synaptic plasticity and cell survival in neurons of the central nervous system. Here, we show that KRas, but not HRas, acutely translocates from the plasma membrane (PM) to the Golgi complex and early/recycling endosomes in response to neuronal activity. Translocation is reversible and mediated by the polybasic-prenyl membrane targeting motif of KRas. We provide evidence that KRas translocation occurs through sequestration of the polybasic-prenyl motif by Ca^{2+}/calmodulin (Ca^{2+}/CaM) and subsequent release of KRas from the PM, in a process reminiscent of GDP dissociation inhibitor–mediated membrane recycling of Rab and Rho GTPases. KRas translocation was accompanied by partial intracellular redistribution of its activity. We conclude that the polybasic-prenyl motif acts as a Ca^{2+}/CaM-regulated molecular switch that controls PM concentration of KRas and redistributes its activity to internal sites. Our data thus define a novel signaling mechanism that differentially regulates KRas and HRas localization and activity in neurons.

Introduction

Ras is a small GTPase that operates as a binary molecular switch between a GDP-bound inactive and GTP-bound active state. Three Ras isoforms, KRas4B (referred hereafter as KRas), NRas, and HRas, encoded by three different genes, are ubiquitously expressed in mammals (Hancock, 2003). Ras activity relies on proper anchoring to the cytoplasmic leaflet of the plasma membrane (PM) by means of a lipid-based PM targeting motif. Such a membrane-anchoring strategy has been adopted by a wide range of signaling proteins (Fivaz and Meyer, 2003) with significant variations in the structure of these motifs (see Table S1, available at http://www.jcb.org/cgi/content/full/jcb.200409157/DC1). The functional relevance of this diversity in membrane anchors remains largely unexplored. The targeting motif of Ras is part of the COOH-terminal hypervariable region, which significantly differs amongst the otherwise highly conserved Ras isoforms. All three Ras isoforms have a CAAX sequence at the COOH terminus that specifies farnesylation and further processing of the COOH-terminal cysteine residue. The targeting motif of KRas contains an additional polybasic region adjacent to the CAAX box, whereas HRas and NRas have palmitoylation site(s) instead (Table S1). These two accessory motifs (polybasic region and palmitoylation) act synergistically with the isoprenyl moiety to target Ras isoforms to the PM (Choy et al., 1999) by apparently distinct mechanisms (Thissen et al., 1997; Apolloni et al., 2000; Roy et al., 2000). It has been proposed that these differences in Ras targeting motifs have a role in generating different signal outputs by differentially regulating subcellular localization or micro-localization within the PM of Ras isoforms (Prior et al., 2001, 2003; Chiu et al., 2002; Bivona et al., 2003).

In addition to an essential role in regulating cell growth and differentiation, Ras signaling has more recently been linked to a wide range of neuronal functions including synaptic and behavioral plasticity (for review see Thomas and Huganir, 2004). Pharmacological and genetic manipulations of the Ras/MAPK cascade provided evidence for a role in learning and memory (Di Cristo et al., 2001; Wu et al., 2001; Kelleher et al., 2004), long-term potentiation (Di Cristo et al., 2001; Kelleher et al., 2004), and other forms of synaptic plasticity (Huang et al., 2000; Wu et al., 2001). Neuronal activation of Ras by membrane depolarization or glutamatergic signaling does not operate "classically" through tyrosine kinases and adaptors, but shows a strong dependence on Ca^{2+} influx through the N-methyl-D-aspartate receptor (NMDA-R) or voltage-gated Ca^{2+} channels (Cullen and Lockyer, 2002). This Ca^{2+}-dependent component

Correspondence to Marc Fivaz: mfivaz@stanford.edu; or Tobias Meyer: Tobias1@stanford.edu

Abbreviations used in this paper: DIV, days in vitro; GDI, GDP dissociation inhibitor; NMDA-R, N-methyl-D-aspartate receptor; PM, plasma membrane; PN, perinuclear; PNS, postnuclear supernatant; RBD, Ras-binding domain of Raf-1.

The online version of this article includes supplemental material.

Supplemental material can be found at:
http://doi.org/10.1083/jcb.200409157

The Journal of Cell Biology, Vol. 170, No. 3, August 1, 2005 429–441
http://www.jcb.org/cgi/doi/10.1083/jcb.200409157

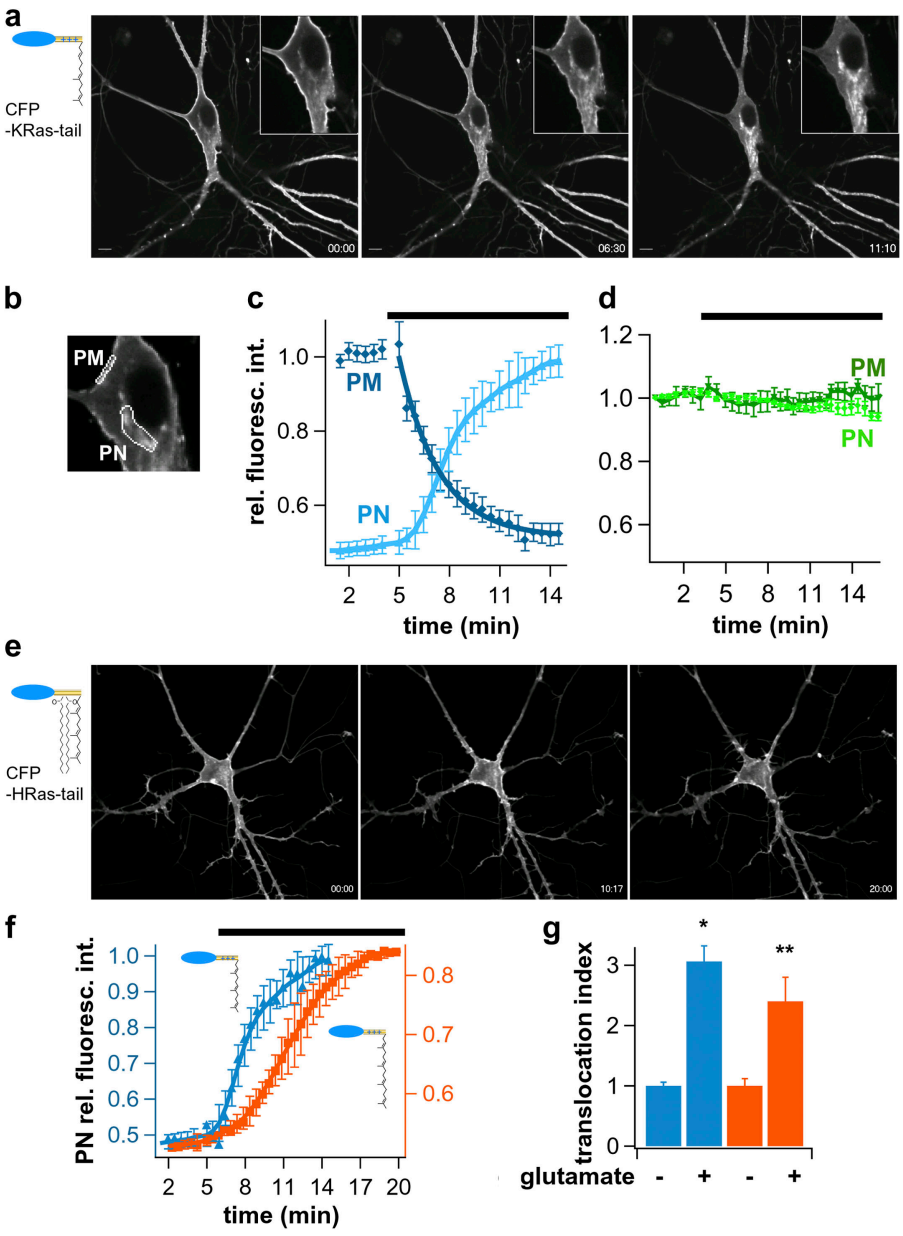

Figure 1. **Activity-induced translocation of CFP-KRas-tail and CFP-Rap1-tail to intracellular membranes.** Hippocampal neurons (12 d in vitro, DIV) transfected with CFP-KRas-tail (a–c, f and g), CFP-HRas-tail (d and e), or CFP-Rap1a-tail (f and g) were stimulated with 50 μM glutamate. (a) Time-lapse images of CFP-KRas-tail redistributing from the PM to a PN compartment. Time is indicated in min and s. Glutamate was added between the first and second image (see Video 1, available at http://www.jcb.org/cgi/content/full/jcb.200409157/DC1). (b) Example of PM and PN regions of interest selected for the translocation analysis. A PM "mask" was generated for each frame in order to take into account cell movements and cell shape changes (see Materials and methods). (c) Average translocation profile of CFP-KRas-tail (n = 25). Plasma membrane (PM, dark blue) and perinuclear (PN, light blue) fluorescence intensities are plotted over time (see Materials and methods). The black bar indicates application of the stimulus. Note that glutamate-induced CFP-KRas-tail release from the PM precedes accumulation of the probe in PN membranes. (d). Average PM and PN levels of CFP-HRas tail plotted over time (n = 15). (e) Time-lapse images of CFP-HRas-tail before (first image) and after glutamate application. (f) Average translocation profile of CFP-Rap1a-tail to PN membranes (orange trace) compared with that of CFP-KRas-tail (blue trace). (g) Histogram quantifying translocation of CFP-KRas-tail (n = 25, blue bars) and Rap1a (n = 7, orange bars). The translocation index refers to the PN to PM intensity ratio and was measured before (−) and after (+) application of glutamate, when PN fluorescence starts to plateau (see Materials and methods) (*, $P < 10^{-6}$; **, $P < 0.01$). Error bars represent the SEM. Bars, 10 μm.

in Ras/MAPK signaling is thought to be important in relaying excitatory synaptic inputs to gene transcription in the nucleus (Dolmetsch et al., 2001), a process required for long-term synaptic remodeling and neuronal survival (Dolmetsch, 2003).

Although considerable evidence points to an essential role of Ras signaling in a variety of neuronal functions, little is known about isoform-specific functions and subcellular localization in neurons. Using a systematic approach to characterize the role of different membrane-anchoring motifs, we here report that the prenyl-polybasic targeting motifs of KRas and Rap1a dictate rapid, reversible and Ca^{2+}-dependent subcellular redistribution in response to glutamatergic signaling. Activity-dependent translocation of KRas to endomembranes is isoform specific and occurs via a shuttling mechanism through the cytoplasm controlled by Ca^{2+}/CaM. We provide evidence that a fraction of KRas relocalized to endomembranes remains in a signaling competent form, suggesting that this activity-dependent translocation process may spatially segregate and modulate KRas and HRas signaling activities in neurons.

Results

Localization of lipid-modified fluorescent probes in hippocampal neurons

In an effort to characterize the function of various PM targeting motifs of signaling proteins in neurons, we designed a panel of PM-targeted fluorescent probes. These probes consist of a diverse set of naturally occurring lipid-based PM targeting motifs (typically 10–20 aa long), tagged either NH_2-terminally or COOH-terminally with EGFP color variants (Table S1). Motifs were selected to ensure that the main known membrane anchor determinants (combinations of different lipids and/or polybasic regions) were represented. Importantly, because these probes lack the functional protein domains (other than the few amino

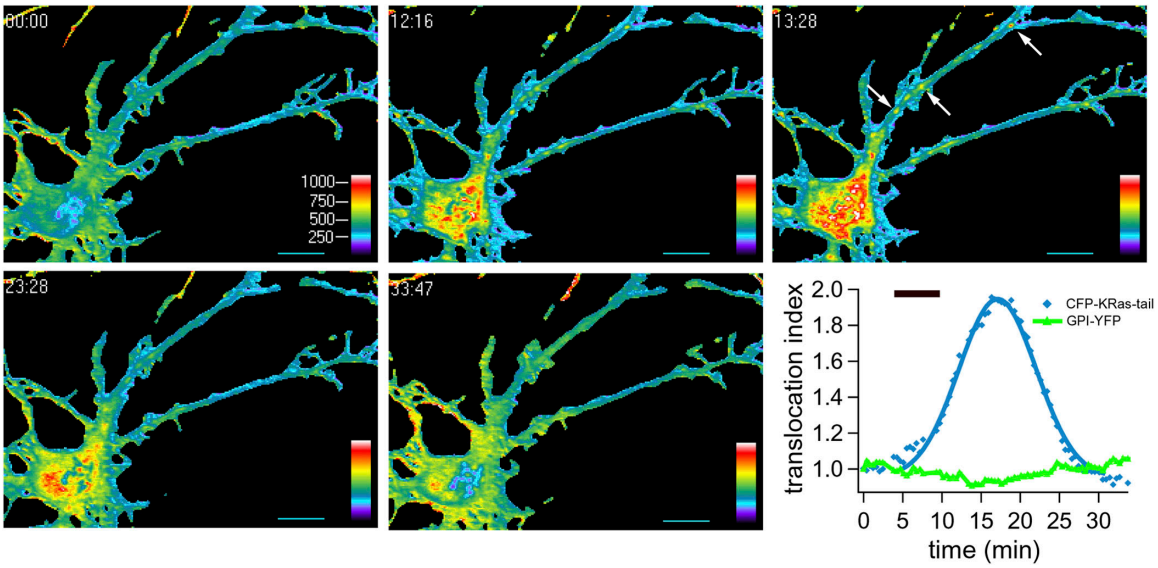

Figure 2. **Reversibility of the CFP-KRas-tail translocation response.** Example of a neuron (DIV 13) coexpressing CFP-KRas-tail and GPI-YFP and stimulated by transient (3 min) application of 25 μM glutamate. Shown are time-lapse ratio images of CFP-KRas-tail over GPI-YFP fluorescence intensity (see Video 2, available at http://www.jcb.org/cgi/content/full/jcb.200409157/DC1). The ratio values are displayed according to a pseudocolor scale (see Materials and methods). CFP-KRas-tail reversibly translocates to PN membranes and peripheral dendritic vesicles (arrows). The time course was quantified by plotting the PM to PN intensity ratio over time (blue trace). As a control, the PM to PN ratio for GPI-YFP is shown in green (PM and PN regions of interest were selected in the cell body). Bars, 10 μm.

acids that are part of the targeting motif), observed differences in subcellular localization are expected to be a direct consequence of their membrane-anchoring motif. We analyzed the distribution of these various probes in hippocampal neurons by confocal microscopy. All probes showed a clear PM localization and varying degrees of intracellular localization (Fig. S1, available at http://www.jcb.org/cgi/content/full/jcb.200409157/DC1).

Neuronal activity triggers reversible translocation of CFP-Kras-tail and CFP-Rap1a-tail to intracellular membranes

We then tested whether the distribution of these probes was sensitive to neuronal activity. Stimulation of hippocampal neurons by bath application of 50 μM glutamate had no effect on their distribution with the exception of CFP-KRas-tail and CFP-Rap1a-tail. Glutamate stimulation led to a striking redistribution of CFP-KRas-tail from the PM to a perinuclear (PN) membrane compartment and dendritic vesicles (Fig. 1 a; Video 1, available at http://www.jcb.org/cgi/content/full/jcb.200409157/DC1). Release of CFP-KRas-tail from the PM occurred throughout the somatodendritic region with fast kinetics ($t_{1/2}$ ~2.5 min) and preceded the accumulation of the probe in intracellular membranes ($t_{1/2}$ ~4.5 min) (Fig. 1, a and c). Interestingly, the CFP-HRas-tail probe (Fig. 1, d and e) did not translocate in response to glutamate. CFP-Rap1a-tail, which exhibits a membrane-interacting motif structurally related to KRas-tail (Table S1), also redistributed intracellularly upon glutamate application. Redistribution was, however, less pronounced (Fig. 1 g) and occurred with slower kinetics (Fig. 1 f). Neuronal activation elicited by NMDA, high K^+ membrane depolarization, or selective stimulation of synaptic NMDA-Rs (Lu et al., 2001) also induced intracellular redistribution of CFP-KRas-tail and CFP-Rap1a-tail, albeit with slightly different kinetics (unpublished data). Importantly, transient application of glutamate (typically a 2–3-min pulse) led to a fully reversible translocation of CFP-KRas-tail (Fig. 2; Video 2) to intracellular vesicles (in the soma and the dendritic arbor) and back to the PM, as shown by a ratiometric analysis using a reference PM marker (see Materials and methods).

Together, these experiments show that the KRas and Rap1a PM targeting motifs regulate translocation of a reporter protein to intracellular membranes in response to neuronal stimulation. As both the KRas and Rap1a motifs consist of a prenyl moiety and a polybasic sequence (and are the only motifs to show this particular combination in our list), these data suggest that this combination represents the minimal membrane-interacting motif that drives translocation.

Cytoplasmic shuttling of the KRas-tail probe to Golgi and early endosomal membranes

Dual color measurements using a Golgi marker (CFP-GalTase) showed that the KRas-tail probe partially colocalizes with the Golgi complex after translocation (Fig. 3 a). Pretreatment with brefeldin A (a fungal metabolite that disrupts the Golgi) only partially inhibited KRas-tail accumulation in PN membranes (Fig. S2, available at http://www.jcb.org/cgi/content/full/jcb.200409157/DC1), suggesting that CFP-KRas-tail also localizes to another juxtanuclear compartment. Consistently, CFP-Kras-tail also partially overlapped with recycling endosomes loaded with Alexa 546–labeled transferrin (alexa546-Tf) (Fig. 4 a). In dendritic processes, KRas-tail clearly redistributed to early endosomes, as shown by colocalization with the early endosome marker $(FYVE)_2$-YFP (Fig. 3 b; Video 3) (Gillooly et al., 2000).

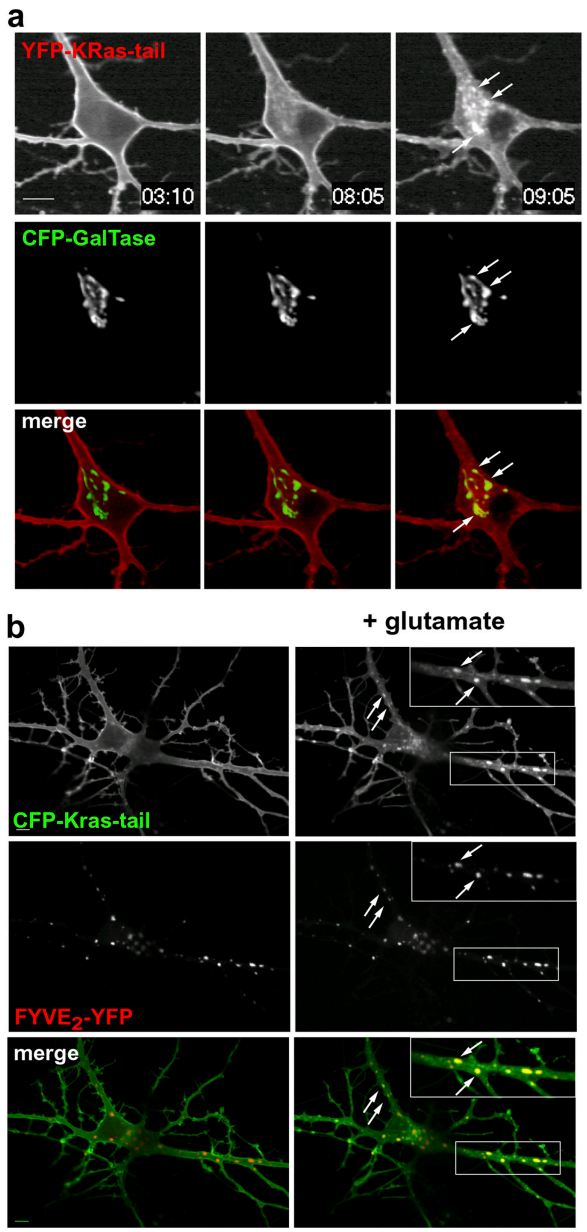

Figure 3. **The Kras-tail probe translocates to Golgi and early endosomal membranes.** Hippocampal neurons were cotransfected with YFP-KRas-tail and CFP-GalTase (a) or CFP-KRas-tail and $FYVE_2$-YFP (b) and stimulated with 50 μM glutamate. (a) Time-lapse images showing YFP-KRas-tail translocating to PN structures that largely overlap with the Golgi marker. Glutamate was added between images 1 and 2. (b) Shown are two time points (before and after glutamate addition) indicating a clear redistribution of CFP-KRas-tail to vesicular structures positive for $FYVE_2$-YFP in dendritic processes (see Video 3, available at http://www.jcb.org/cgi/content/full/jcb.200409157/DC1). Arrows point to KRas-tail–positive stuctures that colocalize with CFP-GalTase (a) or $FYVE_2$-YFP (b). Bars, 10 μm.

We never observed vesicular transport intermediates, but often saw an increased diffuse cytoplasmic staining upon redistribution of CFP-KRas-tail to intracellular organelles (Fig. 1; Video 1). This led us to investigate whether the translocation of CFP-KRas-tail was mediated by vesicular traffic, or instead involved dissociation from the PM and transport/diffusion through the cytoplasm. Consistent with the latter hypothesis, translocation of CFP-Kras-tail was not affected by coexpres-

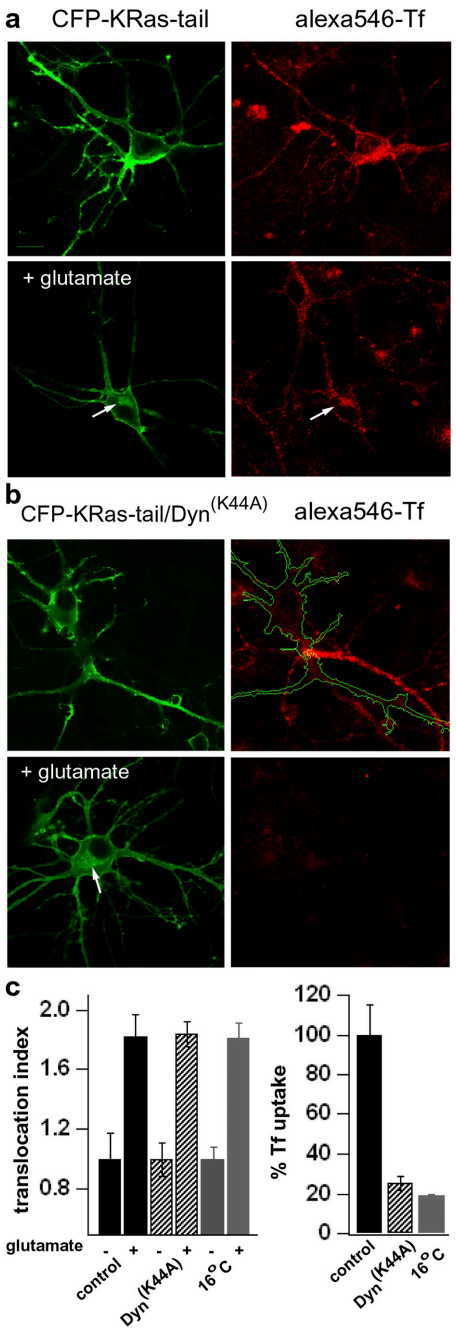

Figure 4. **Translocation of the KRas-tail probe is not an endocytic event.** Hippocampal neurons expressing CFP-KRas-tail (a), or coexpressing CFP-KRas-tail and a dominant-negative mutant of dynamin-1 ($Dyn^{(K44A)}$) (b) were fed with 50 μg/ml alexa546-Tf for 20 min and stimulated (or not) with 50 μM glutamate for 5 min at 37°C. Neurons were then processed for immunocytochemistry and stained with an anti-GFP pAb. (a) Glutamate leads to the accumulation of CFP-KRas-tail in a PN area (arrow) that overlaps with endocytosed alexa546-Tf. (b) Glutamate-induced accumulation of CFP-KRas-tail in PN membranes (arrow) is unaffected by overexpression of $Dyn^{(K44A)}$, despite strong inhibition of alexa546-Tf uptake. (c) Quantification of the effect of $Dyn^{(K44A)}$ or temperature on CFP-KRas-tail translocation and alexa546-Tf uptake. Neither $Dyn^{(K44A)}$ nor lowering of the temperature to 16°C (during alexa546-Tf uptake and glutamate stimulation) affected CFP-KRas-tail translocation, whereas both perturbations reduced Tf uptake >75% in the same cells. Error bars represent the SEM. $n > 20$ for each of these conditions. Bar, 10 μm.

sion of a mutant of dynamin-1 (Dyn^{K44A}) deficient in GTP binding and hydrolysis that efficiently blocks clathrin- (Damke et al., 1994) and caveolae-mediated endocytosis (Oh et al., 1998) (Fig. 4). As a control, we measured transferrin uptake in the same neurons using Alexa 546–labeled transferrin (alexa546-Tf) and found that it was strongly inhibited (Fig. 4). Because some cell surface molecules are endocytosed by a dynamin-independent process, we also blocked membrane traffic by lowering the temperature to 16°C. Although CFP-KRas-tail translocation was not affected under these conditions, transferrin uptake was inhibited >80% (Fig. 4 c). These data indicate that CFP-KRas-tail translocation is unlikely to be an endocytic event, and suggest that translocation occurs via a diffusion-based shuttling mechanism through the cytoplasm.

Full-length KRas exhibits the same translocation response

We then examined whether the full-length CFP-conjugated KRas protein translocates to intracellular membranes in response to glutamate. Fig. 5 (a and b) shows that CFP-KRas undergoes glutamate-induced translocation to PN membranes with kinetics indistinguishable to that of the KRas-tail probe ($t_{1/2}$ ~4.5 min). CFP-tagged constitutively active (Q61L) and dominant-negative (S17N) mutants of KRas redistributed intracellularly with similar kinetics (Fig. 5, a and b), indicating that the translocation process is independent of the nucleotide state of the small GTPase. As observed for the KRas-tail and HRas-tail probes, translocation of the full-length protein occurred for KRas, but not for HRas (Fig. 5, a and c). Together, these results show that the membrane targeting motif of KRas is necessary and sufficient for glutamate-induced translocation of the full-length GTPase, and that translocation is selective for KRas over HRas. An interesting corollary of these data is that neuronal activity leads to a transient spatial segregation of the KRas and HRas isoforms.

Translocation of KRas is a Ca^{2+}-dependent process

We investigated the mechanism by which neuronal activity triggers translocation of CFP-KRas-tail. We found that glutamate-induced translocation was inhibited by AP-5, an NMDA-R antagonist. Absence of extracellular Ca^{2+} also abrogated translocation (Fig. 6 a), indicating that Ca^{2+} influx through the NMDA-R is an obligatory component in this translocation process. These pharmacological manipulations also blocked translocation of (full-length) CFP-KRas (Fig. 6 b). To further analyze the relationship between Ca^{2+} and CFP-KRas-tail translocation, we monitored in parallel KRas-tail-CFP translocation and Ca^{2+} levels (Fig. 6 c), using the C2 domain of PKCγ conjugated to YFP as a calcium sensor (Teruel and Meyer, 2002). Two sequential pulses of glutamate were applied, leading each time to a rapid Ca^{2+} concentration increase (quantified here by a decrease in the YFP-PKCγ-C2 cytoplasmic signal; see legend of Fig. 6 C) followed by a Ca^{2+} decrease to baseline after glutamate washout. Consistent with a direct control of the translocation process by Ca^{2+}, both Ca^{2+} transients were accompanied by reversible accumulation of KRas-tail in PN membranes. Translocation seemed to require high amplitude Ca^{2+} signals because occasionally occurring spontaneous Ca^{2+} transients of typically low amplitude (Fig. 6 c) did not trigger significant translocation of CFP-KRas-tail.

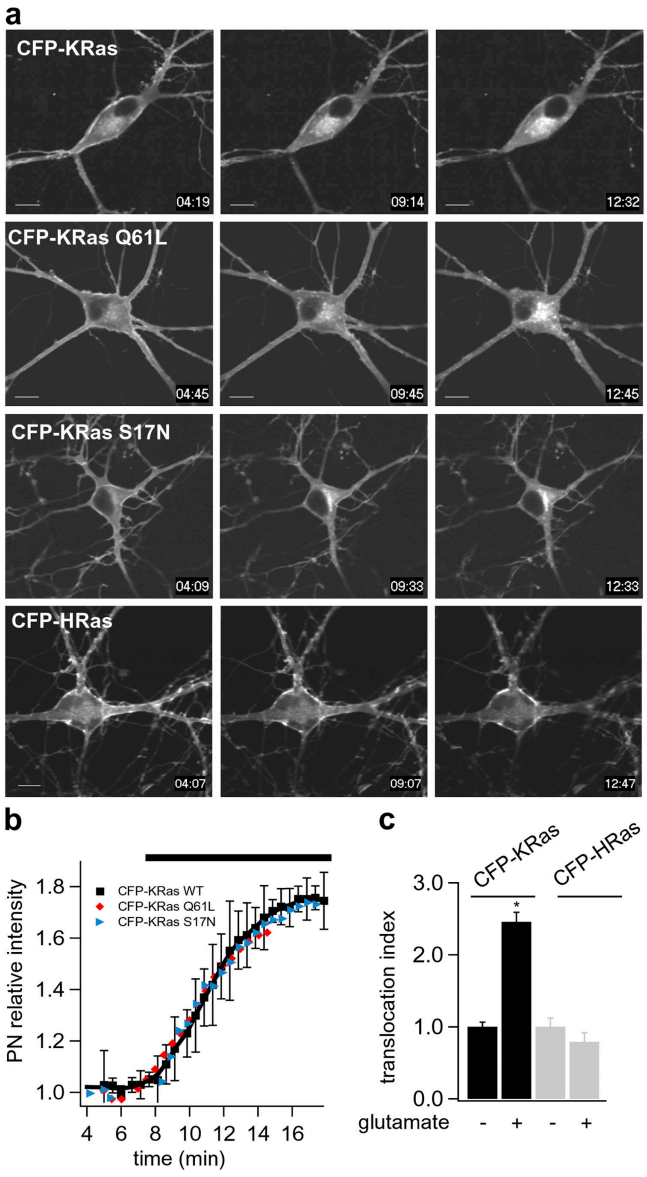

Figure 5. **Translocation of full-length KRas is independent of its nucleotide-binding state.** Hippocampal neurons transfected with CFP-KRas WT, Q61L, and S17N, or HRas, and stimulated with 50 μM glutamate. (a) Representative examples of glutamate-induced translocation of CFP-KRas WT, Q61L, and S17N. Note that CFP-HRas does not redistribute intracellularly in response to glutamate (glutamate was added between the first and second time point). (b) Average translocation profiles for CFP-KRas WT (n = 18), Q61L (n = 15), and S17N (n = 14). Error bars correspond to the SEM, and were omitted for the CFP-KRas Q61L and S17N traces. (c) Quantification of the translocation responses for WT CFP-KRas (n = 18) and CFP-HRas (n = 15). The translocation index refers to the PN/PM intensity ratio. Error bars represent the SEM. (*, $P < 10^{-6}$). Bars, 10 μm.

Translocation of CFP-KRas-tail is regulated by CaM

Our data suggest that activity-dependent Ca^{2+} influx leads to the dissociation of KRas by a mechanism that involves the

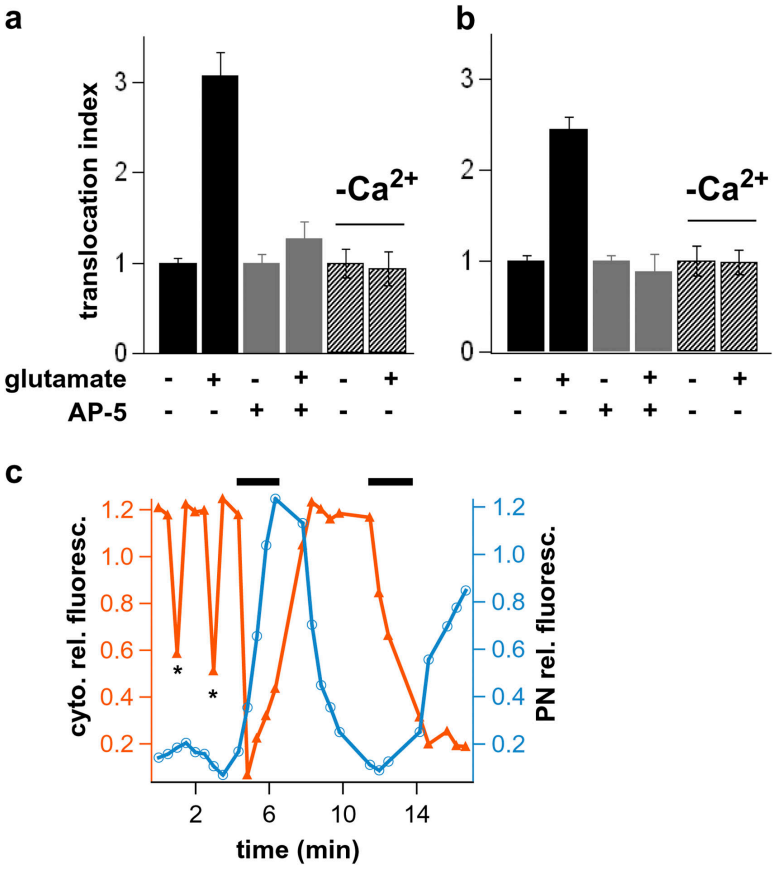

Figure 6. **The stimulus-induced translocation of the Kras membrane interaction motif requires Ca^{2+} signals.** (a and b) Glutamate-induced translocations of CFP-KRas-tail and CFP-KRas are inhibited by the NMDA-R antagonist AP-5 or absence of extracellular Ca^{2+}. (a) CFP-KRas-tail. n = 25, 10, and 8 for control, AP-5, and $-Ca^{2+}$conditions, respectively. ($P < 10^{-5}$ for the control). (b) CFP-KRas. n = 18, 8, and 9 for control, AP-5, and $-Ca^{2+}$ conditions, respectively. ($P < 10^{-6}$ for the control). Error bars represent the SEM. (c) Parallel measurements of glutamate-induced CFP-KRas-tail translocation and Ca^{2+} increase in a neuron cotransfected with YFP-PKCγ-C2. Ca^{2+} increases are monitored by translocation of YFP-PKCγ-C2 from the cytoplasm to the PM. The YFP-PKCγ-C2 intensity profile (orange trace) shows variations of fluorescence intensity in a region of interest selected in the cytoplasm. A decrease in YFP-PKCγ-C2 signal is thus indicative of an increase of intracellular Ca^{2+}. CFP-KRas-tail intensity profile (blue trace) was monitored in the PN region. Two consecutive pulses of glutamate were applied (black bars). Note that CFP-KRas-tail translocation events correlate with glutamate-induced Ca^{2+} increases. The asterisk indicates two spontaneous Ca^{2+} spikes of short duration and low amplitude that did not result in substantial CFP-KRas-tail translocation.

COOH-terminal tail of the small GTPase. We therefore hypothesized that the release of KRas from the PM results from the Ca^{2+}-dependent binding of a cytoplasmic protein to the COOH-terminal tail of KRas, and subsequent destabilization of KRas interactions with the PM. CaM has been shown to interact in a Ca^{2+}-dependent manner with several N-myristoylated proteins, including MARCKS and CAP-23 (Takasaki et al., 1999; Hayashi et al., 2002, 2004; Matsubara et al., 2004). The CaM binding motif was mapped to the lipid modification itself (at the NH_2 terminus of these proteins), as well as to nearby polybasic residues, a motif that is reminiscent of the membrane-targeting domains of KRas and Rap1a (prenylation and polybasic region). Importantly, Ca^{2+}/CaM can displace MARCKS from the PM, indicating a potential role for Ca^{2+}/CaM in regulating reversible membrane interactions. Furthermore, two biochemical studies have reported that Ca^{2+}/CaM binds to KRas (but not HRas) (Villalonga et al., 2001; Sidhu et al., 2003) and dissociates KRas from membranes (Sidhu et al., 2003), although it is not clear from these studies whether CaM interacts with the membrane-anchoring motif or other regions of the small GTPase. This prompted us to investigate whether CaM mediates KRas and Rap1a translocation in neurons by interacting with their membrane anchors. We first assessed whether CaM function was required for CFP-KRas-tail translocation in vivo. Pretreatment of neurons for 10 min with the CaM antagonist w-7 led to ~80% inhibition in CFP-KRas-tail translocation (Fig. 7), providing evidence for a Ca^{2+}/CaM-dependent process.

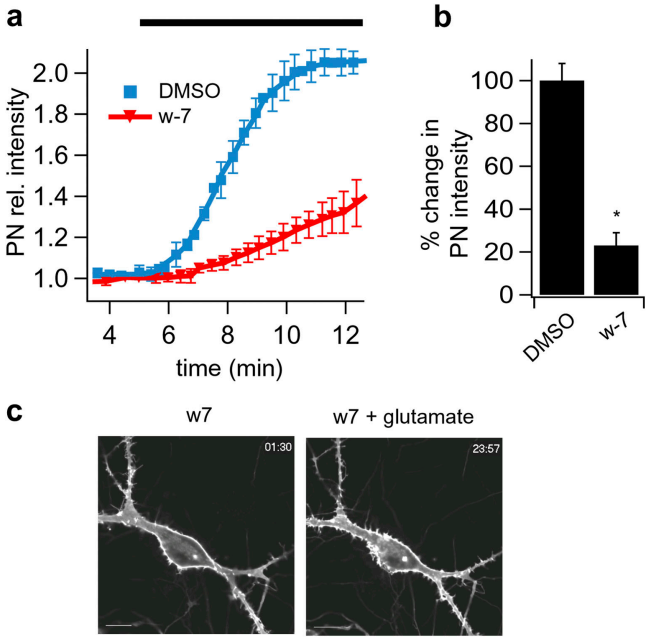

Figure 7. **Translocation is inhibited by the CaM antagonist w-7.** Hippocampal neurons expressing CFP-KRas-tail were treated on stage with DMSO (control) or 30 μM w-7 for 10 min and then were stimulated with 50 μM glutamate in presence of DMSO or w-7. (a) Translocation profiles of CFP-KRas-tail in DMSO- (n = 7) and w-7–treated (n = 18) neurons. (b) Percent change in CFP-KRas-tail PN intensity in w-7 and control cells, at a time point that corresponds to full translocation for the control condition. Error bars correspond to the SEM. (c) An example of CFP-KRas-tail localization in w-7–treated cells before and ~15 min after glutamate addition. Bars, 10 μm (*, $P < 10^{-4}$).

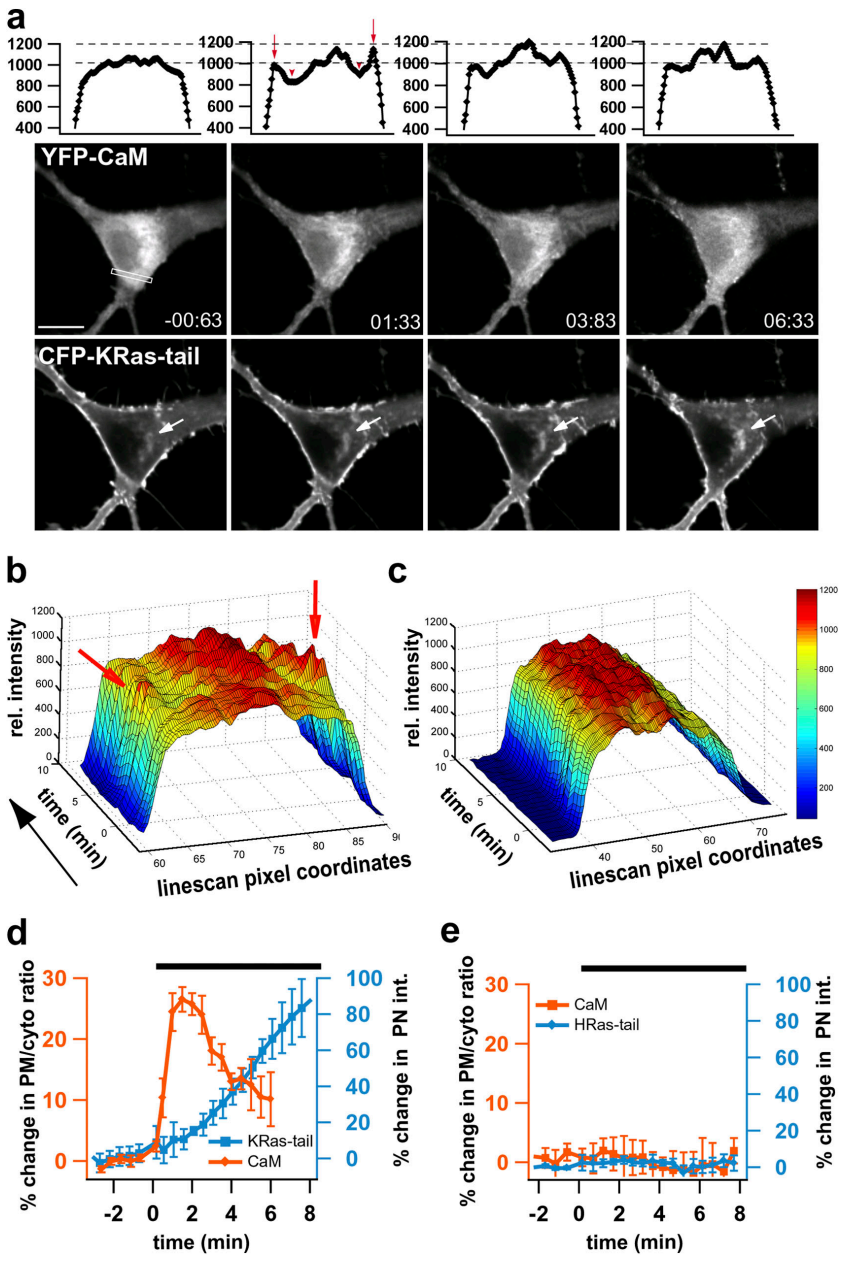

Figure 8. **CaM interacts with the COOH-terminal tail of KRas in an activity-dependent manner.** Hippocampal neurons cotransfected with YFP-CaM and either CFP-KRas-tail (a, b, and d) or CFP-HRas-tail (c). (a) Addition of glutamate at t = 0 leads to transient recruitment of YFP-CaM to the PM in cells coexpressing CFP-KRas-tail. A line scan across the cell soma (white rectangle) shows transient recruitment of YFP-CaM to the PM (red arrows) and concomitant decrease in intensity in the cytoplasm (red arrowheads). CFP-KRas-tail translocation to PN membranes (white arrows) occurs with slower kinetics. (b) Surface plot displaying the line scan intensity profile of YFP-CaM (in panel a) as a function of time (see Materials and methods). The red arrows indicate translocation to the PM after glutamate addition (t = 0). See Fig. S3 for other examples (available at http://www.jcb.org/cgi/content/full/jcb.200409157/DC1). (c) Line scan surface plot of YFP-CaM in a cell coexpressing CFP-HRas-tail. Glutamate (added at t = 0) does not induce YFP-CaM translocation to the PM. The images from which that surface plot is derived are shown in Fig. S4 together with other examples. (d) Average translocation profile of CaM in KRas-tail–expressing neurons (*n* = 7). A translocation response was observed in all cells analyzed. The orange trace shows percent change in the PM to cytoplasm intensity ratio as a function of time. The PM and cytoplasm intensity values are derived from the line scan profile and are read at positions corresponding to the "peak" and "valley" (shown in panel a) by the red arrows and arrowheads respectively. (e) A similar analysis for CaM in HRas-tail–expressing neurons shows no sign of translocation (*n* = 9). None of the cells analyzed in panel e showed any translocation response. The blue traces indicate percent change of intensity in the PN area for KRas-tail (d) and HRas-tail (e). Error bars represent the SEM. Bar, 10 μm.

Activity-dependent interaction of CaM with the COOH-terminal tail of KRas

To assess whether CaM interacts in vivo with CFP-KRas-tail in an activity-dependent manner, hippocampal neurons were cotransfected with CFP-KRas-tail and YFP-CaM and stimulated with glutamate. Before stimulation YFP-CaM localized diffusively throughout the cytoplasm, with a preferential distribution in the PN area in some neurons (Fig. 8 a, first panel). Within a minute after glutamate addition, YFP-CaM translocated to the PM (Fig. 8 a). YFP-CaM recruitment to the PM was transient, and followed by CFP-KRas-tail translocation to PN membranes. A line scan analysis across the cell soma shows a modest but unambiguous recruitment of YFP-CaM to the cell edges (Fig. 8 a, red arrows) with a concomitant decrease in the cytoplasm (red arrowheads), indicative of a relocalization of CaM to the PM. A surface plot representation of line scans across the time-lapse sequence (see Materials and methods) shows a sharp increase in fluorescence intensity at the PM after glutamate addition (at t = 0) followed by a slower decay to near-basal levels (Fig. 8 b) (see Fig. S3 for other examples; available at http://www.jcb.org/cgi/content/full/jcb.200409157/DC1). We did not observe translocation of YFP-CaM to the PM in neurons cotransfected with CFP (unpublished data) or CFP-HRas-tail (Fig. 8 c; Fig. S4), indicating that YFP-CaM translocation to the PM is KRas-tail dependent. This last result also implies that we do not detect YFP-CaM recruitment to endogenous KRas, presumably because of high levels of CaM expression, relative to KRas (see end of paragraph). We also often measured a relatively modest increase in CaM fluorescence in the PN area upon glutamate addition (see line scans and surface plots in Fig. 8, a–c, and Figs. S3 and S4). This effect was, however, also observed in neurons cotransfected with CFP (unpublished data) or the HRas-tail probe, and

is therefore not specifically mediated by the KRas membrane-interacting motif. Fig. 8 d shows the average translocation profile of CaM in KRas-tail–expressing cells, which precedes translocation of KRas-tail to PN membranes, whereas no translocation of CaM is observed in neurons expressing the HRas-tail probe (Fig. 8 e). We repeatedly observed only partial translocation of CaM to the PM in KRas-tail–expressing cells, possibly because of high endogenous levels of CaM (relative to exogenous YFP-CaM and CFP-KRas-tail) that could compete with exogenous YFP-CaM for CFP-KRas-tail binding sites at the PM. Consistent with this hypothesis, we measured the relative levels of expression of exogenous and native CaM, using an anti-CaM antibody, and found that exogenously introduced CaM only increases overall CaM levels by ~15% (Fig. S5). Together, these data are consistent with rapid binding of CaM to the KRas membrane-interacting motif and a subsequent release of KRas from the PM upon stimulation.

Ca^{2+}/CaM binds and dissociates CFP-KRas-tail and CFP-Rap1a-tail from membranes

To test more directly the mechanism by which CaM triggers KRas translocation, we examined whether CaM interacts with the COOH-terminal tail of KRas in a pull-down assay. CaM beads were incubated in the presence of Ca^{2+} with postnuclear supernatants (PNS) from HeLa cells expressing CFP-KRas-tail or CFP-HRas-tail. A Western blot analysis shows efficient and Ca^{2+}-dependent binding of CFP-KRas-tail to CaM beads (Fig. 9 a). The HRas-tail probe, however, was not retained on the beads, nor was β-tubulin, indicating isoform-selective and specific interaction of the KRas COOH-terminal tail with Ca^{2+}/CaM. A similar biochemical approach showed that CaM also interacts with the COOH-terminal tail of Rap1a, in a Ca^{2+}-dependent manner (Fig. 9 a). To determine whether the lipid modification is directly involved in CaM binding, we designed a mutant of CFP-KRas-tail that lacks a functional CaaX box (an alanine residue was substituted to the prenylated cysteine). CFP-KRas-tail$^{(C261A)}$ showed a strong decrease in affinity for Ca^{2+}/CaM (Fig. 9 a) compared with CFP-KRas-tail wt, suggesting the prenyl modification itself is part of the binding motif.

To test whether Ca^{2+}/CaM binding to the COOH-terminal tail of KRas and Rap1a leads to membrane dissociation, we incubated PNS of cells expressing CFP-KRas-tail, CFP-Rap1a-tail, or CFP-HRas-tail with (or without) purified CaM, in the presence of Ca^{2+} or EGTA, and separated membranes from the cytosol by high speed ultracentrifugation. A Western blot analysis shows significant redistribution of both the KRas-tail and Rap1a-tail probes, but not the HRas-tail probe, from the membrane to the soluble fraction in presence of Ca^{2+}/CaM (Fig. 9 b). Ca^{2+} was again required because CaM did not extract these two probes in the presence of EGTA.

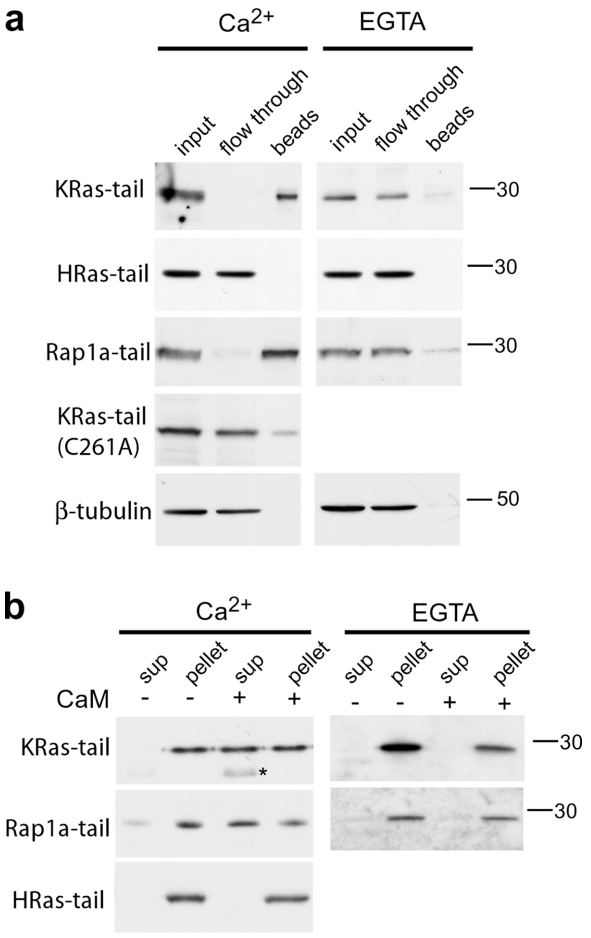

Figure 9. **Ca^{2+}/CaM binds and dissociates CFP-KRas-tail and CFP-Rap1a-tail from membranes.** (a) PNS of HeLa cells expressing CFP-KRas-tail, CFP-HRas-tail, CFP-Rap1a-tail, or CFP-KRas-tail (C261A) were incubated with CaM beads in the presence of Ca^{2+} or EGTA. Input, flow through (unbound material), and beads were analyzed by immunoblotting using an anti-GFP or anti-β-tubulin antibody. (b) A PNS of CFP-KRas-tail–, CFP-Rap1a-tail–, or CFP-HRas-tail–expressing HeLa cells was treated (or not) with purified CaM in the presence of Ca^{2+} or EGTA and submitted to high speed centrifugation. The supernatant (cytosol) and pellet (membranes) fractions were immunoblotted against GFP. Note that CaM leads to a significant redistribution of a CFP-KRas-tail and CFP-Rap1a-tail from membranes to the cytosol in a Ca^{2+}-dependent manner, but did not extract CFP-HRas-tail from membranes. In each experiment, 100% of the recovered supernatant and pellet fractions were loaded on the gel. Shown are representative examples for each of these experiments, which have been repeated at least three times. The asterisk indicates a soluble protein that is picked up by the anti-GFP antibody and corresponds presumably to a minor fraction of GFP that is not coupled to the prenyl modification.

Intracellular redistribution of KRas activity in response to glutamatergic signaling

Finally, to investigate the role of KRas translocation in neuronal Ras signaling, we made use of a fluorescent reporter for active, GTP-bound Ras. The probe consists of the Ras-binding domain (RBD) of Raf-1 fused to CFP (RBD-CFP) (Chiu et al., 2002). When cotransfected with YFP-KRas, RBD-CFP localized diffusively in the cytoplasm in resting cells (Fig. 10 a, first panel). Addition of 50 μM NMDA triggered recruitment of RBD-CFP to the PM (Fig. 10 a) within tens of seconds, indicating rapid activation of Ras in response to neuronal activity. Recruitment of RBD-CFP to the PM did not occur in cells expressing RBD-CFP only (unpublished data), consistent with the previous observation that the RBD probe is not sensitive enough to report endogenous activation of Ras (Chiu et al., 2002). As YFP-KRas translocated to PN membranes, RBD-CFP

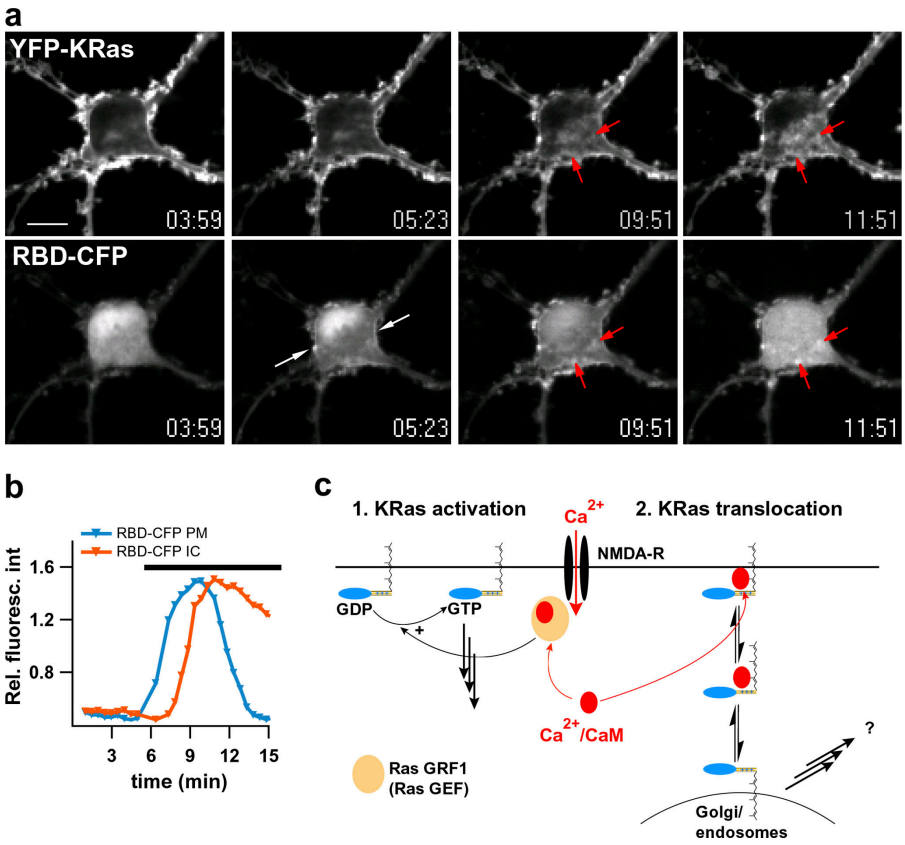

Figure 10. **KRas activity redistributes to intracellular membranes upon neuronal stimulation.** (a) An example of a hippocampal neuron (DIV 15) cotransfected with YFP-KRas and RBD-CFP (Ras-binding domain of Raf-1 fused to CFP) and stimulated with 50 μM NMDA (added between frame 1 and 2). NMDA induces a rapid recruitment of RBD-CFP from the cytoplasm to the PM (white arrows), followed by translocation of YFP-KRas and concomitant redistribution of RBD-CFP to intracellular membranes (red arrows). Bar, 10 μm. (b) Quantification of RBD-CFP translocation to the PM (blue trace) and intracellular compartments (IC, orange trace) shown in panel a. Recruitment of RBD-CFP to internal sites is delayed and prolonged compared with translocation to the PM. (c) An integrated model for Ras signaling and KRas translocation at the synapse (see last paragraph in the Discussion section).

redistributed and colocalized with intracellular structures positive for YFP-KRas (Fig. 10 a), indicating that a fraction of translocated KRas remained in a GTP-bound, signaling-competent form after it translocated to internal membranes. The recruitment of RBD to intracellular compartments was delayed compared with recruitment to the PM and persisted even after most of YFP-KRas (and RBD-CFP) had left the PM (Fig. 10 b), suggesting that KRas translocation leads to sustained internal KRas activity in response to neuronal stimulation.

Discussion

By screening a panel of diverse lipid-based PM targeting motifs we have identified a novel neuronal signaling mechanism that regulates PM levels of proteins with a polybasic-prenyl targeting motif. We found that this minimal motif acts as sensor of sustained neuronal activity and triggers rapid and reversible relocalization of KRas to intracellular compartments in a Ca^{2+}-dependent process. Our results indicate that this translocation event occurs via cytoplasmic shuttling rather than vesicular transport, and are in support of a mechanism that involves sequestration of the polybasic-prenyl motif and subsequent extraction of the small GTPase by Ca^{2+}/CaM from the PM. Due to its different membrane-anchoring motif, HRas does not interact with Ca^{2+}/CaM and is not subject to this dynamic regulation. Our data therefore unravel a striking difference in KRas and HRas dynamics in neurons, which is strictly mediated by their distinct membrane-anchoring motifs. Finally, we show that activity-dependent translocation of KRas may serve as a way to quickly and selectively carry persistent KRas activity to intracellular membranes, providing a regulatory mechanism that allows differential control of the spatial and temporal activity patterns of KRas and HRas.

Activity-dependent reversible membrane interactions mediated by the polybasic-prenyl membrane targeting motif

Prenyl-based PM targeting motifs of Ras-like small GTPases are generally viewed as stable, nonregulated PM anchors, unlike other lipid modifications such as S-palmitoylation or N-myristoylation, which can reversibly interact with membranes (for reviews see Ames et al., 1997; Bijlmakers and Marsh, 2003; Fivaz and Meyer, 2003). Our work now shows that prenylation, in the context of an adjacent polybasic region, can reversibly transfer proteins from the PM to intracellular membranes within minutes, indicating that prenyl-based membrane interactions are more dynamic than previously envisioned. Reversible membrane interactions of KRas in neurons is in agreement with studies showing that KRas can dissociate from membranes in vitro (Leventis and Silvius, 1998; Roy et al., 2000).

Reversible membrane interactions via a Ca^{2+}/CaM-regulated lipid-dependent switch

Our work indicates that reversible membrane interactions mediated by the PM targeting motifs of KRas and Rap1a is regulated by Ca^{2+}/CaM. First, CaM binds to the COOH-terminal membrane anchors of KRas and Rap1a (but not Hras) and pulls

these probes off the membrane in vitro (Fig. 9, a and b). Second, glutamate stimulation leads to recruitment of Ca^{2+}/CaM to the COOH-terminal tail of KRas at the PM, before KRas translocation (Fig. 8). Finally, KRas-tail translocation in vivo is inhibited by the CaM antagonist w-7 (Fig. 7). Together, these results support the notion that Ca^{2+}/CaM sequesters the polybasic-prenyl motif of KRas and Rap1a and extracts these small GTPases from the PM. The observed difference in kinetics of translocation between CFP-KRas-tail and CFP-Rap1a-tail may reflect the difference in length between the farnesyl (C15) and generanylgeranyl (C20) lipid moieties (the longer lipid anchor presumably confers more affinity for the PM). Destabilization of this membrane interaction by Ca^{2+}/CaM could result from disruption of electrostatic interactions between the polybasic region and negatively charged phospholipids of the PM and/or direct hydrophobic interactions of Ca^{2+}/CaM with the prenyl group (see below). A role of CaM as a modulator of reversible protein–membrane interactions has been previously described for the myristoylated alanine-rich C kinase substrate (MARCKS) protein. The polybasic effector domain of MARCKS interacts electrostatically with acidic lipids (Rusu et al., 2004) and is a good substrate for Ca^{2+}/CaM. Binding of Ca^{2+}/CaM to the effector domain pulls the peptide off membranes (Arbuzova et al., 1997). By analogy with this switch mechanism initially put forward by McLaughlin and Aderem (1995), we would like to propose that the polybasic-prenyl targeting motif of KRas and Rap1a acts as a molecular switch that controls reversible membrane interactions of KRas and Rap1a through Ca^{2+}/CaM.

What is the Ca^{2+}/CaM binding site in the COOH-terminal tails of KRas and Rap1a? The polybasic region is reminiscent of a class of Ca^{2+}/CaM-binding motifs that consists of a high density of basic residues (~50% of the sequence) alternating with hydrophobic residues (MARCKS is an example of this basic Ca^{2+}/CaM-binding motif [Aderem, 1992; Yamauchi et al., 2003]). However, there is no hydrophobic residue in the COOH-terminal tail of KRas, and only one valine residue in the COOH-terminal tail of Rap1a (see Table S1). Because hydrophobic interactions are central to Ca^{2+}/CaM target recognition (Yamniuk and Vogel, 2004), we believe it is unlikely that the polybasic domain of KRas and Rap1a acts as a Ca^{2+}/CaM-binding motif on its own. Within the last few years, several N-myristoylated proteins have been shown to interact with Ca^{2+}/CaM, defining a novel potential CaM-binding motif (Takasaki et al., 1999; Hayashi et al., 2002, 2004; Matsubara et al., 2003, 2004). A recent crystal structure of CAP23/NAP bound to CaM revealed that the myristoyl moiety penetrates in the Ca^{2+}-exposed hydrophobic groove of CaM (Matsubara et al., 2004), in a way reminiscent of the hydrophobic pocket of Rho-GDI for isoprenylated cdc42 (Gosser et al., 1997). Consistent with a direct role of the prenyl moiety in CaM recognition, we found that substitution of the prenylated cysteine to an alanine in the CaaX motif significantly reduced binding of CFP-KRas-tail to Ca^{2+}/CaM (Fig. 9 a).

The inability of HRas to interact with Ca^{2+}/CaM could be due to the absence of a polybasic region and (or) the presence of additional palmitoyl modifications that are unlikely to fit in the Ca^{2+}/CaM hydrophobic pocket. Because Ca^{2+}/CaM binding to the COOH-terminal tail of KRas and Rap1a does not seem to rely on a particular amino acid sequence, but rather on the presence of a polybasic-prenyl combination, Ca^{2+}/CaM-mediated reversible membrane interactions may potentially apply to a sizable subgroup of small GTPases and other proteins. In support of this prediction, CaM has been shown to interact in vitro with a number of small GTPases that exhibit a polybasic-prenyl motif, such as Rab3A (Park et al., 1997), Rab3B (Sidhu and Bhullar, 2001), RalA (Wang et al., 1997), RalB (Clough et al., 2002), and KRas (Sidhu et al., 2003. In addition, CaM has also been reported to dissociate Rab3A (Park et al., 1997; Villalonga et al., 2001) and KRas (Sidhu et al., 2003) from membranes in vitro.

Ca^{2+}/CaM-dependent translocation of KRas: a process related to GDI function

Ca^{2+}/CaM-mediated retrieval of KRas and Rap1a from the PM bears some similarities with GDP dissociation inhibitor (GDI)–mediated recycling of Rab and Rho family members (Wu et al., 1996; Olofsson, 1999). Ca^{2+}/CaM, like GDI, extracts small GTPases from membranes and presumably shields the prenyl moiety from the hydrophilic environment of the cytoplasm. Ca^{2+}/CaM-mediated reversible translocation of KRas to the Golgi is therefore conceptually analogous to recycling of Rab GTPases from a target to a donor membrane compartment during one cycle of vesicular traffic. However, whereas GDI operates on the inactive GDP-bound form of the GTPase only, CaM function is triggered by Ca^{2+}, and is therefore independent of the nucleotide state of the small GTPase (Fig. 5). Whether CaM also plays a role in unloading KRas onto intracellular membranes is presently unknown.

Recycling of CFP-KRas-tail back to the PM

We have shown that upon transient glutamate stimulation, CFP-KRas-tail translocation to intracellular membranes is fully reversible (Fig. 2), and that recycling of CFP-KRas-tail back to the PM correlates with a return of Ca^{2+} to basal levels (Fig. 6 c). One plausible interpretation of these data is that upon Ca^{2+} decrease, CaM releases from the KRas tail, allowing the probe to recycle back from the intracellular membranes to the PM. The mechanism of transport back to the PM may share some similarities with delivery of newly synthesized KRas to the PM.

Newly synthesized Ras isoforms (i.e., KRas, NRas, and HRas) are first delivered to ER/Golgi membranes where maturation of the prenyl modification proceeds, through endoproteolytic removal of −AAX, and carboxymethylation of the COOH-terminal isoprenylcysteine (Choy et al., 1999; Fu and Casey, 1999). Targeting of matured Ras to the PM relies on accessory signals; palmitoylation for HRas/NRas and a polybasic region for KRas (Choy et al., 1999; Roy et al., 2000). Intriguingly, whereas HRas/NRas delivery to the PM occurs via vesicular transport through the secretory pathway, KRas targeting to the PM operates via a yet-undefined, presumably nonvesicular pathway (Thissen et al., 1997; Apolloni et al., 2000; Silvius, 2002), possibly by simple diffusion down an electrostatic gra-

dient (greater negative charge density at the PM, relative to intracellular membranes), where PM targeting would be essentially driven by electrostatic interactions of the KRas polybasic domain with negatively charged phospholipids. Likewise, the polybasic region of KRas (now free of Ca^{2+}/CaM) may be responsible for recycling the small GTPase from intracellular membranes back to the PM via a similar mechanism.

Activity-dependent translocation of KRas: implications for neuronal Ras signaling

Work by Chiu et al. (2002) and Bivona et al. (2003) has shown that in fibroblasts, T cells, and PC12 cells, ER/Golgi-localized HRas signaling is engaged in response to growth receptors or T cell receptor activation at the PM. In their study, activation of HRas in the Golgi was shown to be the result of a Ca^{2+}- and PLCγ1- dependent recruitment of the Ras guanine nucleotide exchange factor RasGRP1 to Golgi membranes (Bivona et al., 2003). We have now identified an alternative mechanism by which Ras signaling can be carried to intracellular membranes in response to neuronal excitatory inputs. In this case, the presence of active, GTP-bound KRas in endomembranes relies on Ca^{2+}/CaM-dependent translocation of KRas, rather than activation of prelocalized HRas by a diffusible messenger.

A model that integrates translocation of KRas and Ras/MAPK signaling at a glutamatergic synapse is shown in Fig. 10 c. Activity-dependent Ca^{2+} influx through the NMDA-R or L-type voltage-gated Ca^{2+} channels (unpublished data) leads to rapid (within seconds) Ras activation at the PM by means of Ca^{2+}- or Ca^{2+}/CaM-dependent Ras GEFs (Krapivinsky et al., 2003). KRas (but not HRas) then undergoes Ca^{2+}/CaM-dependent translocation to endomembranes (within minutes) and further engages signaling processes from intracellular sites. One speculative role of KRas translocation, in the context of activity-dependent gene transcription, would be to facilitate the relay of local Ca^{2+} elevations in dendritic spines to the nucleus by localizing the MAPK pathway in closer proximity to the nucleus.

In conclusion, we have identified what is to our knowledge the first example of a signaling-induced translocation of a Ras family member. The mechanisms that underlie this translocation process are potentially applicable to a number of other signaling proteins, and may provide a molecular and cellular basis for signaling specificity of a variety of lipid-modified signaling molecules in neurons.

Materials and methods

Plasmid constructs

Double-stranded oligonucleotides encoding the membrane targeting motifs of a panel of lipid-modified proteins (Table S1) were cloned into the pECFP-N1 or pEYFP-N1 and pECFP-C1 or pEYFP-C1 expression vectors (CLONTECH Laboratories, Inc.) for NH_2-terminal and COOH-terminal lipid modifications, respectively (oligonucleotides and restrictions sites available on request). All constructs were sequenced before use. The human CFP-KRas, CFP-KRas(Q61L), and CFP-HRas(S17N) constructs were previously described (Heo and Meyer, 2003) and were gifts from Won Do Heo (Stanford University, Stanford, CA). The RBD-CFP constructs were obtained by cloning a PCR product encoding the RBD of human Raf-1 (bp 280–522) into the pECFP-N1 vector and was a gift from Cecile Arrieumerlou (Stanford University, Stanford, CA). The CaM constructs and GPI-YFP were gifts from Mary Teruel (Stanford University, Stanford, CA) and Patrick Keller (Max Planck Institute of Molecular Cell Biology and Genetics, Dresden, Germany). The CFP-GalTase construct was purchased from CLONTECH Laboratories, Inc. The YFP-PKCγ-C2 construct is described elsewhere (Teruel and Meyer, 2002). The $FYVE_2$-GFP is a gift from H. Stenmark (The Norwegian Radium Hospital, Oslo, Norway). The tandem FYVE domain was cloned into the N2-YFP vector from CLONTECH Laboratories, Inc.

Cell culture transfection

Rat hippocampal neurons were prepared as previously described (Fink et al., 2003). Neurons were transfected at 7 d in vitro (DIV) using LipofectAMINE 2000 (Invitrogen) according to the manufacturer's instructions and imaged between DIV 10 and DIV 15. HeLa cells were cultured in DME (GIBCO BRL) in 10% FCS and transfected with FuGENE (Roche) according to the manufacturer's instructions.

Live-cell confocal microscopy and immunocytochemistry

Live-cell dual color measurements were performed on a spinning-disc confocal microscope. CFP and YFP excitations were obtained by the 442-nm line of a helium-cadmium laser (100 mM; Kimmon Electrics) and the 514-nm line of an argon laser (300 mW; Melles Griot), respectively. The beams of the two lasers were merged onto a beam combiner dichroic (Chroma Technology Corp.), homogenized with a holographic laser diffuser and focused into the confocal scan head (Yokogawa, McBain) equipped with a dual CFP/YFP dichroic and mounted on the side port of an inverted microscope (model IX-71; Olympus). Fluorescence was recorded at 480 nm (CFP) and 530 nm (YFP) with bandpass (40-nm half-bandwith) and longpass interference filters, respectively, mounted in a Lambda 10-2 filter wheel (Sutter Instrument Co.). Images were captured with a CCD camera (Cool SNAP HQ; Roper Scientific), driven by MetaMorph 6.1 (Universal Imaging Corp.). Neurons were imaged in extracellular buffer EB (25 mM Hepes, pH 7.40, 150 mM NaCl, 1.3 mM $CaCl_2$, 1.3 mM $MgCl_2$, 5 mM KCl, and 33 mM glucose) on a heated stage (33-35C), using a 40× (NA 1.35) objective. Neurons were processed for immunocytochemistry as described elsewhere (Fink et al., 2003). In brief, neurons were fixed in 4% PFA and 4% sucrose, and were permeabilized with 0.l% Triton X-100 for 5 min. The polyclonal anti-GFP (Molecular Probes, Inc.) and monoclonal anti-CaM (Upstate Biotechnology) antibodies were revealed using Alexa 488– and Alexa 546–labeled secondary antibodies, and neurons were imaged using a PASCAL 5 laser scanning confocal microscope (Carl Zeiss MicroImaging, Inc.).

Image processing

See online supplemental material.

Pharmacological treatments

Neurons were stimulated with 50 μM glutamate or NMDA in EB containing 5 μM glycine. Membrane depolarization was triggered by 100 μM KCl for 3 min. 50 μM AP-5 (Sigma-Aldrich) was used to block the NMDA-R. The CaM antagonist w-7 (Sigma-Aldrich) was used at a 30-μM final concentration for 10 min.

CaM binding assay

PNS were prepared from HeLa cells expressing lipid-modified fluorescent probes. Cells were homogenized in 250 mM sucrose, 3 mM imidazole (pH 7.4) by passage through a 22G injection needle, and a PNS was obtained after a 10-min spin at 2,500 rpm. PNS were then incubated with CaM sepharose 4B beads (GE Healthcare) for 1 h at 4°C, in 50 mM Tris-HCl, pH 6.8, 50 mM NaCl, and 0.5% Triton X-100, in the presence of 1.3 mM Ca or 2 mM EGTA. Unbound material was removed by a quick centrifugation step. Beads were washed twice, and bound material was eluted by boiling beads in sample buffer. Input and flow-through fractions were precipitated with $CHCl_3$/MeOH and analyzed together with the beads by SDS-PAGE (12.5%), transferred onto a polyvinylidene difluoride membrane (Bio-Rad Laboratories), and immunoblotted using an anti-GFP antibody (Molecular Probes, Inc.) or an anti-β-tubulin mAb. The HRP-conjugated secondary antibody (Jackson ImmunoResearch Laboratories) was revealed with the SuperSignal chemiluminescent substrate (Pierce Chemical Co.).

Membrane dissociation assay

We used a modified version of the protocol described by Park et al. (1997). A PNS of HeLa cells, expressing CFP-KRas-tail or CFP-Rap1a-tail (20 μg of proteins) was incubated with or without 40 μg purified CaM (Immunochemicals) in 50 mM Tris-HCl, pH 7.4, 0.5 mM $MgCl_2$, 0.5 mM $CaCl_2$, and 1 mM DTT, for 1 h at 37°C, and was fractionated by ultracen-

trifugation (50,000 rpm; for 30 min at 4°C). The resulting supernatant and membrane pellet were immunoblotted using an anti-GFP antibody as described above.

Online supplemental material

Table S1 lists lipid-modified fluorescent probes used in this work. Fig. S1 shows distribution of lipid-modified probes in hippocampal neurons. Fig. S2 depicts translocation of YFP-KRas-tail in BFA-treated neurons. Fig. S3 shows additional examples of CaM translocation to the PM in KRas-tail–expressing neurons. Fig. S4 depicts additional examples showing lack of CaM translocation in HRas-tail–expressing neurons. Fig. S5 shows a comparison of endogenous CaM and exogenous CFP-CaM expression levels.

We thank Annette Salmeen, Mike Bradshaw, Thierry Galvez, Ricardo Dolmetsch, Gisou Van der Goot, and Isabelle Le Blanc for critical reading of the manuscript. We are grateful to Maddy Craske for help in neuron cultures and to John Hancock for insightful comments.

M. Fivaz is a fellow of the "Fonds National Suisse pour la recherche scientifique." This work is supported by National Institutes of Health grant MH64801 (to T. Meyer).

Submitted: 27 September 2004
Accepted: 24 June 2005

References

Aderem, A. 1992. The MARCKS brothers: a family of protein kinase C substrates. *Cell.* 71:713–716.

Ames, J.B., R. Ishima, T. Tanaka, J.I. Gordon, L. Stryer, and M. Ikura. 1997. Molecular mechanics of calcium-myristoyl switches. *Nature.* 389:198–202.

Apolloni, A., I.A. Prior, M. Lindsay, R.G. Parton, and J.F. Hancock. 2000. H-ras but not K-ras traffics to the plasma membrane through the exocytic pathway. *Mol. Cell. Biol.* 20:2475–2487.

Arbuzova, A., J. Wang, D. Murray, J. Jacob, D.S. Cafiso, and S. McLaughlin. 1997. Kinetics of interaction of the myristoylated alanine-rich C kinase substrate, membranes, and calmodulin. *J. Biol. Chem.* 272:27167–27177.

Bijlmakers, M.J., and M. Marsh. 2003. The on-off story of protein palmitoylation. *Trends Cell Biol.* 13:32–42.

Bivona, T.G., I. Perez De Castro, I.M. Ahearn, T.M. Grana, V.K. Chiu, P.J. Lockyer, P.J. Cullen, A. Pellicer, A.D. Cox, and M.R. Philips. 2003. Phospholipase Cγ activates Ras on the Golgi apparatus by means of RasGRP1. *Nature.* 424:694–698.

Chiu, V.K., T. Bivona, A. Hach, J.B. Sajous, J. Silletti, H. Wiener, R.L. Johnson II, A.D. Cox, and M.R. Philips. 2002. Ras signalling on the endoplasmic reticulum and the Golgi. *Nat. Cell Biol.* 4:343–350.

Choy, E., V.K. Chiu, J. Silletti, M. Feoktistov, T. Morimoto, D. Michaelson, I.E. Ivanov, and M.R. Philips. 1999. Endomembrane trafficking of ras: the CAAX motif targets proteins to the ER and Golgi. *Cell.* 98:69–80.

Clough, R.R., R.S. Sidhu, and R.P. Bhullar. 2002. Calmodulin binds RalA and RalB and is required for the thrombin-induced activation of Ral in human platelets. *J. Biol. Chem.* 277:28972–28980.

Cullen, P.J., and P.J. Lockyer. 2002. Integration of calcium and Ras signalling. *Nat. Rev. Mol. Cell Biol.* 3:339–348.

Damke, H., T. Baba, D.E. Warnock, and S.L. Schmid. 1994. Induction of mutant dynamin specifically blocks endocytic coated vesicle formation. *J. Cell Biol.* 127:915–934.

Di Cristo, G., N. Berardi, L. Cancedda, T. Pizzorusso, E. Putignano, G.M. Ratto, and L. Maffei. 2001. Requirement of ERK activation for visual cortical plasticity. *Science.* 292:2337–2340.

Dolmetsch, R. 2003. Excitation-transcription coupling: signaling by ion channels to the nucleus. *Sci. STKE.* 2003:PE4.

Dolmetsch, R.E., U. Pajvani, K. Fife, J.M. Spotts, and M.E. Greenberg. 2001. Signaling to the nucleus by an L-type calcium channel-calmodulin complex through the MAP kinase pathway. *Science.* 294:333–339.

Fink, C.C., K.U. Bayer, J.W. Myers, J.E. Ferrell Jr., H. Schulman, and T. Meyer. 2003. Selective regulation of neurite extension and synapse formation by the beta but not the alpha isoform of CaMKII. *Neuron.* 39:283–297.

Fivaz, M., and T. Meyer. 2003. Specific localization and timing in neuronal signal transduction mediated by protein-lipid interactions. *Neuron.* 40:319–330.

Fu, H.W., and P.J. Casey. 1999. Enzymology and biology of CaaX protein prenylation. *Recent Prog. Horm. Res.* 54:315–342; discussion 342–343.

Gillooly, D.J., I.C. Morrow, M. Lindsay, R. Gould, N.J. Bryant, J.M. Gaullier, R.G. Parton, and H. Stenmark. 2000. Localization of phosphatidylinositol 3-phosphate in yeast and mammalian cells. *EMBO J.* 19:4577–4588.

Gosser, Y.Q., T.K. Nomanbhoy, B. Aghazadeh, D. Manor, C. Combs, R.A. Cerrione, and M.K. Rosen. 1997. C-terminal binding domain of Rho GDP-dissociation inhibitor directs N-terminal inhibitory peptide to GTPases. *Nature.* 387:814–819.

Hancock, J.F. 2003. Ras proteins: different signals from different locations. *Nat. Rev. Mol. Cell Biol.* 4:373–384.

Hayashi, N., M. Matsubara, Y. Jinbo, K. Titani, Y. Izumi, and N. Matsushima. 2002. Nef of HIV-1 interacts directly with calcium-bound calmodulin. *Protein Sci.* 11:529–537.

Hayashi, N., C. Nakagawa, Y. Ito, A. Takasaki, Y. Jinbo, Y. Yamakawa, K. Titani, K. Hashimoto, Y. Izumi, and N. Matsushima. 2004. Myristoylation-regulated direct interaction between calcium-bound calmodulin and N-terminal region of pp60v-src. *J. Mol. Biol.* 338:169–180.

Heo, W.D., and T. Meyer. 2003. Switch-of-function mutants based on morphology classification of Ras superfamily small GTPases. *Cell.* 113:315–328.

Huang, Y.Y., K.C. Martin, and E.R. Kandel. 2000. Both protein kinase A and mitogen-activated protein kinase are required in the amygdala for the macromolecular synthesis-dependent late phase of long-term potentiation. *J. Neurosci.* 20:6317–6325.

Kelleher, R.J., III, A. Govindarajan, H.Y. Jung, H. Kang, and S. Tonegawa. 2004. Translational control by MAPK signaling in long-term synaptic plasticity and memory. *Cell.* 116:467–479.

Krapivinsky, G., L. Krapivinsky, Y. Manasian, A. Ivanov, R. Tyzio, C. Pellegrino, Y. Ben-Ari, D.E. Clapham, and I. Medina. 2003. The NMDA receptor is coupled to the ERK pathway by a direct interaction between NR2B and RasGRF1. *Neuron.* 40:775–784.

Leventis, R., and J.R. Silvius. 1998. Lipid-binding characteristics of the polybasic carboxy-terminal sequence of K-ras4B. *Biochemistry.* 37:7640–7648.

Lu, W., H. Man, W. Ju, W.S. Trimble, J.F. MacDonald, and Y.T. Wang. 2001. Activation of synaptic NMDA receptors induces membrane insertion of new AMPA receptors and LTP in cultured hippocampal neurons. *Neuron.* 29:243–254.

Matsubara, M., K. Titani, H. Taniguchi, and N. Hayashi. 2003. Direct involvement of protein myristoylation in myristoylated alanine-rich C kinase substrate (MARCKS)-calmodulin interaction. *J. Biol. Chem.* 278:48898–48902.

Matsubara, M., T. Nakatsu, H. Kato, and H. Taniguchi. 2004. Crystal structure of a myristoylated CAP-23/NAP-22 N-terminal domain complexed with Ca^{2+}/calmodulin. *EMBO J.* 23:712–718.

McLaughlin, S., A. Aderem. 1995. The myristoyl-electrostatic switch: a modulator of reversible protein-membrane interactions. *Trends Biochem Sci.* 20:272–276.

Oh, P., D.P. McIntosh, and J.E. Schnitzer. 1998. Dynamin at the neck of caveolae mediates their budding to form transport vesicles by GTP-driven fission from the plasma membrane of endothelium. *J. Cell Biol.* 141:101–114.

Olofsson, B. 1999. Rho guanine dissociation inhibitors: pivotal molecules in cellular signalling. *Cell. Signal.* 11:545–554.

Park, J.B., C.C. Farnsworth, and J.A. Glomset. 1997. Ca^{2+}/calmodulin causes Rab3A to dissociate from synaptic membranes. *J. Biol. Chem.* 272: 20857–20865.

Prior, I.A., A. Harding, J. Yan, J. Sluimer, R.G. Parton, and J.F. Hancock. 2001. GTP-dependent segregation of H-ras from lipid rafts is required for biological activity. *Nat. Cell Biol.* 3:368–375.

Prior, I.A., R.G. Parton, and J.F. Hancock. 2003. Observing cell surface signaling domains using electron microscopy. *Sci. STKE.* 2003:PL9.

Roy, M.O., R. Leventis, and J.R. Silvius. 2000. Mutational and biochemical analysis of plasma membrane targeting mediated by the farnesylated, polybasic carboxy terminus of K-ras4B. *Biochemistry.* 39:8298–8307.

Rusu, L., A. Gambhir, S. McLaughlin, and J. Radler. 2004. Fluorescence correlation spectroscopy studies of Peptide and protein binding to phospholipid vesicles. *Biophys. J.* 87:1044–1053.

Sidhu, R.S., and R.P. Bhullar. 2001. Rab3B in human platelet is membrane bound and interacts with Ca^{2+}/calmodulin. *Biochem. Biophys. Res. Commun.* 289:1039–1043.

Sidhu, R.S., R.R. Clough, and R.P. Bhullar. 2003. Ca^{2+}/calmodulin binds and dissociates K-RasB from membrane. *Biochem. Biophys. Res. Commun.* 304:655–660.

Silvius, J.R. 2002. Mechanisms of Ras protein targeting in mammalian cells. *J. Membr. Biol.* 190:83–92.

Takasaki, A., N. Hayashi, M. Matsubara, E. Yamauchi, and H. Taniguchi. 1999. Identification of the calmodulin-binding domain of neuron-specific protein kinase C substrate protein CAP-22/NAP-22. Direct involvement of protein myristoylation in calmodulin-target protein interaction. *J. Biol. Chem.* 274:11848–11853.

Teruel, M.N., and T. Meyer. 2002. Parallel single-cell monitoring of receptor-triggered membrane translocation of a calcium-sensing protein module. *Science.* 295:1910–1912.

Thissen, J.A., J.M. Gross, K. Subramanian, T. Meyer, and P.J. Casey. 1997. Pre-

nylation-dependent association of Ki-Ras with microtubules. Evidence for a role in subcellular trafficking. *J. Biol. Chem.* 272:30362–30370.

Thomas, G.M., and R.L. Huganir. 2004. MAPK cascade signalling and synaptic plasticity. *Nat. Rev. Neurosci.* 5:173–183.

Villalonga, P., C. Lopez-Alcala, M. Bosch, A. Chiloeches, N. Rocamora, J. Gil, R. Marais, C.J. Marshall, O. Bachs, and N. Agell. 2001. Calmodulin binds to K-Ras, but not to H- or N-Ras, and modulates its downstream signaling. *Mol. Cell. Biol.* 21:7345–7354.

Wang, K.L., M.T. Khan, and B.D. Roufogalis. 1997. Identification and characterization of a calmodulin-binding domain in Ral-A, a Ras-related GTP-binding protein purified from human erythrocyte membrane. *J. Biol. Chem.* 272:16002–16009.

Wu, G.Y., K. Deisseroth, and R.W. Tsien. 2001. Spaced stimuli stabilize MAPK pathway activation and its effects on dendritic morphology. *Nat. Neurosci.* 4:151–158.

Wu, S.K., K. Zeng, I.A. Wilson, and W.E. Balch. 1996. Structural insights into the function of the Rab GDI superfamily. *Trends Biochem. Sci.* 21:472–476.

Yamauchi, E., T. Nakatsu, M. Matsubara, H. Kato, and H. Taniguchi. 2003. Crystal structure of a MARCKS peptide containing the calmodulin-binding domain in complex with Ca^{2+}-calmodulin. *Nat. Struct. Biol.* 10:226–231.

Yamniuk, A.P., and H.J. Vogel. 2004. Calmodulin's flexibility allows for promiscuity in its interactions with target proteins and peptides. *Mol. Biotechnol.* 27:33–57.

Fivaz et al. http://www.jcb.org/cgi/doi/10.1083/jcb.200409157

Supplemental materials and methods

Image processing
Image analysis was performed using MetaMorph 6.1 on 12-bit background-subtracted images

Quantification of plasma membrane (PM) fluorescence
We applied a set of operations to accurately monitor PM variations in intensity by taking into account cell movements and shape changes that may occur during imaging. In brief, a confocal plane that shows a well-defined ring of PM fluorescence around the cell body was chosen. Images in a stack were thresholded, binarized, and eroded using built-in MetaMorph functions. A PM mask was generated for each frame by subtracting the eroded stack of images from the original binarized stack and combining the resulting stack with the unprocessed stack of images, using the logical "AND" function. The average fluorescence intensity of a selected region of interest (ROI) was then logged onto an Excel spreadsheet, normalized, and plotted over time using Igor 5.0 software (WaveMetrics).

Quantification of perinuclear (PN) fluorescence
Accumulation of fluorescent probes in a perinuclear (PN) region was quantified by drawing a ROI in the PN area after glutamate-induced translocation and measuring the average intensity in that ROI over time.

Translocation index
The extent of glutamate-induced translocation was often represented as the PN-to-PM intensity ratio. In histogram representations, the PN-to-PM ratio was arbitrarily set to 1 before stimulation.

Dual-color ratio imaging
Probe-specific translocation of CFP-KRas-tail over GPI-YFP was visualized by dividing images in the CFP channel by those in the YFP channel. The resulting stack was multiplied by an arbitrary factor (500) and background pixels were removed by combining this processed stack of images with a binary mask of the cell using the logical "AND" function. Ratio values are displayed according to a pseudocolor scale.

Line scans and surface plots
A line-scan approach was used to quantify CaM recruitment to the PM. A line was positioned across the cell soma in a region where PM fluorescence of the KRas-tail or HRas-tail probe at the cell edges was obvious before stimulation. Line scans across a stack of images were normalized to account for global loss of fluorescence intensity. Each pixel value was divided by the sum of all pixels along the line and multiplied by an arbitrary factor (10,000). Surface plots were generated using the surf (X, Y, Z) function in MatLab7.1, where X, Y, and Z are two-dimensional matrices representing pixel coordinates of the line scan, time, and intensity values, respectively.

For presentation purposes, the range of gray values displayed in an image (or a stack of images) was adjusted in MetaMorph before images were converted to an 8-bit format and pasted in Adobe Illustrator without further processing. The gamma factor was set to 1 for all images shown.